Incremental growth of normal faults: Insights from a laser-equipped analog experiment

A. Schlagenhauf, Isabelle Manighetti, J. Malavieille, S. Dominguez

Incremental growth of normal faults: insights from a laser-equipped analog experiment

Aloé Schlagenhauf [a,b,*], Isabelle Manighetti [a], Jacques Malavieille [b], Stéphane Dominguez [b]

[a] *Laboratoire de Géophysique Interne et Tectonophysique (LGIT), CNRS, Observatoire de Grenoble (OSUG), Université J. Fourier, Maison des Géosciences, BP 53, 38041 Grenoble cédex 9, France.*

[b] *Géosciences Montpellier, UMR 5243, CNRS, Université Montpellier 2, Place E. Bataillon, 34095 Montpellier cédex 05, France.*

* Corresponding author. Correspondence address: LGIT, Maison des Géosciences, BP 53, 38041 Grenoble cédex 9, France. Tel.: (+33) 476.63.51.70; fax: (+33) 476.63.52.52

E-mail addresses: aloe.schlagenhauf@obs.ujf-grenoble.fr (A. Schlagenhauf); isabelle.manighetti@obs.ujf-grenoble.fr (I. Manighetti); jacques.malavieille@gm.univ-montp2.fr (J. Malavieille); stephane.dominguez@gm.univ-montp2.fr (S. Dominguez).

Abstract

We conducted a laser-equipped analog experiment aimed at quasi-continuously monitoring the growth of a dense population of normal faults in homogeneous conditions. To further understand the way geological faults progressively gain in slip and length as they accumulate more strain, we measured with great precision the incremental slip and length changes that the analog faults sustain as they grow. These measurements show that the analog faults share common features with the natural ones. In particular, during their growth, the faults develop and maintain cumulative slip profiles that are generally triangular and asymmetric. The growth takes place through two distinct phases: an initial, short period of rapid lateral lengthening, followed by a longer phase of slip accumulation with little or no lengthening. The incremental slip is found to be highly variable in both space (along the faults) and time, resulting in variable slip rates. In particular, 'short- and long-term' slip rates are markedly different. We also find that slip measurements at local points on fault traces do not contain clear information on the slip increment repeat mode. Finally, while the fault growth process is highly heterogeneous when considered at the scale of a few slip events, it appears homogeneous and self-similar at longer time scales which integrate many slip increments. This is likely to be the result of a feedback between stress heterogeneities and slip development. The long-term scale homogeneity also implies that the long-term faulting process is primarily insensitive to the short-term heterogeneities that are rapidly smoothed or redistributed. We propose a new conceptual scenario of fault growth that integrates the above observations and we suggest that faults grow in a bimodal way as a result of a self-driven and self-sustaining process.

Keywords: Fault growth, analog modeling, normal faults, slip profiles, slip increments

1- Introduction

Faults generally grow, that is, accumulate slip and lengthen, through the repetition of earthquakes. Yet, how such a growth occurs is still unclear as we lack data documenting how earthquake slip events repeat on faults. Consequently, fundamental questions such as 'Do repeating earthquake slip events have similar amplitudes and lengths? Does any major slip event on a fault contribute to its further lengthening? How do repeating earthquake slips relate to cumulative displacements on long-term faults?' are still unanswered. We have only sparse information, arising partly from rare observations, and partly from models.

Paleoseismological data show that, in some cases, the paleo-slip events have followed at regular time intervals with similar amplitudes and lengths (e.g., Rockwell et al., 2001; Klinger et al., 2003; Haibing et al., 2005). This suggests that faults may grow by accumulating constant slip without lengthening. Yet, in other cases, the paleo-earthquakes are found to have occurred at irregular time intervals and to have been dissimilar in size and location (e.g., Weldon et al., 2004; Palumbo et al., 2004; Daeron et al., 2005). This behavior is a sign of greater complexities in the fault growth process. On the other hand, the analyses of long-term faults whose cumulative displacements are the sum of hundreds to thousands of earthquakes (e.g., Taylor et al., 2004) generally provide little information on those past earthquakes. They thus fail to establish a link between repeat of earthquake slip events and fault growth.

Contrasting with the scarcity of data is our capacity of producing models and qualitative scenarios depicting how faults may grow. These are rooted in *a priori* hypotheses, such as faults behaving as simple, narrow, elastic cracks with no cohesion, linear elastic behavior of the crust, and elastic rebound theory (e.g., Scholz, 2002 for a review). The community interested in earthquakes provides numerical models that describe how earthquake slip events repeat on faults depending on the level of stress/strain being accumulated and relaxed (e.g. Shimazaki and Nakata, 1980), and on some other parameters such as friction on the fault plane (e.g. Tse and Rice, 1986; Rice and Ben-Zion, 1996). These models are useful as they can be directly compared with real earthquake slip data. By contrast, they are never compared with long-term slip measurements, so they do not provide any link between repeat of earthquake slip events and fault growth. On the other hand, the community more interested in overall fault behavior provides qualitative scenarios and more rarely numerical models that describe how faults may grow over long time spans (10^4-10^7 yrs; Segall and Pollard, 1980; Walsh and Watterson, 1987; 1988; Peacock and Sanderson, 1991; Marrett and Allmendinger, 1991; Cowie and Scholz, 1992a, 1992b; Bürgmann et al., 1994; Cartwright et al. 1995;

Willemse et al., 1996; Cowie, 1998; Cowie and Roberts, 2001; Walsh et al., 2002; Kim and Sanderson, 2005). These scenarios are useful for comparison with real long-term slip measurements, but they are rarely confronted with earthquake slip data or with earthquake mechanics. They do therefore also fail to provide a link between repeat of earthquake slip events and fault growth.

Our objective is to explore an alternative field between observation of natural faults and developments of *ad hoc* models. We aim at examine and better understand how slip increments follow in space and time on a fault to make it grow. We address that topic through an analog experiment that allows for a large number of normal faults to form and grow under homogeneous conditions, while their surface lengths and slips are measured quasi-continuously with an interferometric laser system. Although this approach does not reproduce the earthquake process, it sheds light upon the way faults progressively gain in slip and length as they accommodate more strain. Note that, while many analog models have already been produced to simulate fault development (with a particular focus on normal faults; e.g. Horsfield, 1977; Faugeres and Brun, 1984; Ackermann et al., 2001), with a few of them being monitored (Mansfield and Cartwright, 2001; Bellahsen et al., 2003; Marchal et al., 2003; Bellahsen and Daniel, 2005), this is the first time that the incremental fault growth is measured quasi-continuously, and at such a high resolution. This is also the first time the analysis is carried out with a sufficiently dense population of incremental slip events to identify common properties.

2- Experimental protocol

2.1- Experimental design and scaling

We study normal faults because their displacements can be easily measured at the model surface. Since we seek identifying general, intrinsic properties of the fault growth process, we need make the faults developing in the absence of any local complexity. Heterogeneous stress boundary conditions, variations of material properties, influence of preexisting discontinuities, etc… are as many factors -not systematic in nature- that may indeed modify the fault growth process (e.g. Bürgmann et al., 1994; Buiter and Schreurs, 2006). To avoid such possible effects, we have developed a new analog protocol that allows normal faults to be formed and grown in a homogeneous material and a homogeneous stress field. It is important to note that most available analog models do not fulfill the later condition (details in supporting online material A). We adopt, with some modifications, the approach developed

by Schreurs et al. (2002). The model is constructed on top of a thick foam bar that has been previously shortened by compression. The foam bar is then let to progressively 'decompress', which transfers a continuous, homogeneous extension over the width of the overlying model. For reasons explained in many papers (e.g., Hubbert, 1937; Davy and Cobbold, 1991; Lallemand and Malavieille, 1992; Lohrman et al., 2003; Buiter and Schreurs, 2006), dry quartz sand is used to approximate the brittle crust. The one we use is 98.5% made of SiO2, has a mean density of 2.1, and a mean grain size of 112 μm. The scaling factor that results is $1\text{-}2.10^{-5}$ (1 cm in the model represents 1-2 km in the field). Since we want to produce a large number of growing faults, the model does not include any basal material such as silicone putty that would make strain localizing onto a few large faults only (e.g. Davy et al., 1995; Bellahsen et al., 2003).

The apparatus is presented in supporting online material B. In a first step, the foam bar is compressed by 25% between two metallic jaws. Then a 8 cm-thick layer of sand is deposited on top of the compressed foam. The model is sprinkled with a thin powder (25% silica, 74% sand, and 1% black rubber dust; not a rheological interface) aimed at increasing its surface cohesion while allowing 'ground reference points' to be defined. Then the foam bar is progressively decompressed from operating back the two jaws; the decompression transfers extension to the overlaying sand layer. The plastic-made elastic sidewalls of the apparatus avoid longitudinal extension to develop in the sand cake, so that the strain field imposed at the base of the model is homogeneous in its central part (i.e., between the jaws), and decreases to zero on either side. Our study only focuses on the model central part (frame, Fig.1).

Note that we have repeatedly performed the above experiment to ensure the strength of the results that we describe below. We have in particular varied the thickness of the sand cake; that of 8 cm revealed to be a good compromise between the number of faults being produced and the height of their surface escarpments.

2.2- Measurements

Measurements were performed at each 1 mm-decompression step, hence quasi-continuously. Yet, for clarity and brevity reasons, we only describe results at each 1 cm-step. In total, we decompressed the bar by 12 such steps, making the foam still slightly compressed by the end of the experiment. The total experiment corresponds to having stretched the sand model by 20%, by successive steps of 1.7%.

First, numerical high-resolution pictures were taken with a camera at each 1 mm-extension step. The combination of these pictures allows the space-time evolution of the faults to be

visualized quasi-continuously (supporting movie, online material C). Second, the model was equipped with an interferometric laser system allowing accurate (pixel size 0.3 mm) digital elevation models (DEM) of the sand surface to be constructed at each step. The laser system operates as standard Radar Interferometry (e.g., Bürgmann et al., 2000) and is described in Graveleau and Dominguez, 2008. Twelve DEMs were constructed to monitor the evolution of the model topography at every 1 cm step of extension. From each DEM, we extracted elevation profiles following the top and base of the fault scarps. Where a fault trace had several closely spaced strands at the same along-strike position, the extracted profiles were made to include them. From the top and base profiles, we calculated the variation of vertical displacement along strike. The faults have steep scarps ($\geq 60°$) so that those vertical displacements approximate the actual fault slips. Results were then plotted as strike-parallel vertical projections for analysis (Fig.2). Overall, about 100 faults formed and evolved in the interior of the central frame (Fig.1). We restricted our analysis to the largest ones. A few faults initiated in the central frame and propagated outside of it. We considered only those that ended hardly beyond the frame. In total, we thus analyzed a population of 30 faults, synthetic and antithetic, representing a total of 250 incremental slip profiles.

2.3- Errors

Most faults have lengths that rapidly (at most, over the first third of the experiment) became greater than twice the thickness of the sand layer, which they thus cut through. We are thus confident that the 2D measurements of lengths and displacements performed at the model surface are representative of the 3D fault evolution at depth, at least over the last two thirds of the experiment.

Errors on the measurements have multiple sources. The largest likely arises from the hand-extraction of the elevation profiles, particularly during the first stages of growth when fault traces are tenuous. The smallest slips that we could distinctly measure in the first stages of the experiment are 0.1-0.15 mm, and happened to be on faults a few cm-long. Also, the granular nature of the sand introduces a roughness of ≈ 0.1 mm. The calibration of the laser introduces a periodic noise in the DEMs, having an amplitude and a wavelength of 0.25 and 10 mm, respectively. We removed that noise by slightly filtering the slip profiles (supporting online material D). From the combination of the errors above, we estimate that fault length and slip are determined with a maximum error of a few mm and of 0.1-0.15 mm, respectively, over most of the experiment but the very first stages. In those first stages (at most, stages 1-4), fault length may be underestimated by a few cm.

3- Data analysis

The experiment is presented as a movie in supporting online material C. Most faults start forming surface traces soon after extension has begun. Faults initiate evenly over the central section of the model, which confirms that the extensional stress field is homogeneous. Fault traces evolve from tenuous zones of dilatance in the first stages, to topographic escarpments that grow higher and longer as extension increases. In the following, we define 'fault initiation' as the stage when vertical displacements become resolvable at the surface (stages 3 or 4, at most 5% extension). 'Slip' and 'displacement' are used similarly. Maximum displacement is noted D_{max}. A 'slip increment' (or 'slip event') is the slip-length change recorded by a fault at the model surface as the model sustains an additional 1 cm-step of extension. 'Slip rate' is used to describe the displacement accumulated over a specific time span.

3a- Overall shape of the slip profiles

As they grow, faults develop slip profiles that generally have a well-defined envelope shape (Fig.2). Two types of shapes are most commonly observed, that of a symmetric triangle (Fig. 2a-b-c) and that of a strongly asymmetric triangle (Fig. 2d-e-f). A few more complex shapes are found; yet they generally arise from the evolution of triangular shapes (supporting online material E). These more complex shapes have in common to exhibit high slip gradients at both tips. In some cases, faults maintain the same overall shape as they grow (ex: Fig. 2a-b-d-f); in other cases, the shape of the slip profile changes as the fault grows: although still triangular overall, it shifts from symmetric to asymmetric (ex: Fig. 2c-e) or vice-versa. This shows that the position of the maximum displacement may vary in time along a fault (Fig.3). While the slip profiles show any degree of asymmetry in the very first stages of growth (Fig.3 and supporting online material F-a), they pertain to only two categories, symmetric or asymmetric, in the last stages (supporting online material F-b). Commonly, asymmetry and high slip gradient develop where a growing fault meets another, generally oblique or antithetic fault (supporting online material C).

3b- Fault lengthening versus slip increase - overall behavior

Figure 4 and supporting online material G show the evolution of fault lengths as a function of time. About 45% of the faults (black, Fig.4) initiate with a 'short' length generally less than

half their final length, then rapidly lengthen laterally in the following few stages so that, at 30% of the experiment, they have reached a length almost as long as their final one. About 50% of the faults (grey, Fig.4) conversely initiate with a length more than half their final length, then hardly lengthen further laterally over the whole experiment. Note that, because fault lengths may be underestimated in the very first stages of the experiment, the 50% value is a minimum. Finally, two faults (dotted grey, Fig.4) initiate with a length averaging their half final length, then hardly lengthen during most of the experiment but at the very last stages when they resume lengthening. Together these show that at least 80% of the faults achieved 70% or more of their final length in the first third of the faulting history. This demonstrates that faults grow in two distinct, successive phases. They sustain an initial phase when they essentially gain in length and this occurs rapidly; then they sustain a subsequent period when they go on growing without much lengthening.

Whether they are lengthening or not, faults accumulate vertical slip (Fig.5a). The variation of maximum displacement versus time plots roughly as a straight line for each fault (Fig.5b), suggesting a roughly regular vertical growth. The fan-looking distribution of the D_{max}-Time curves further suggests that the vertical growth is more or less rapid depending on which fault is concerned; the shortest faults seem to be those most slowly increasing in slip (Fig.5a). When variations of D_{max} are scaled to fault size (Fig.6), they appear roughly similar for all faults but the smallest ones. Hence, although it occurs at different rates, and although the locus of maximum slip may move over time along the faults, the vertical growth, here taken as the progressive increase in D_{max}, is homogeneous and regular overall.

Figure 7 depicts how the ratio of maximum displacement over length (D_{max}/L) varies as the faults lengthen. When faults are in a stage of rapid lengthening (Fig.7a), their D_{max}/L ratio keeps roughly constant, on the order of $1\text{-}2.10^{-3}$. By contrast, when faults are in a stage of slip accumulation with little or no lengthening (Fig.7b), their D_{max}/L ratio increases as the faults accumulate more slip (up to one order of magnitude). It results that the D_{max}/L ratios spread a broad range of values when the whole fault population is considered over the whole time of the experiment (supporting online material H). Faults with triangular profiles (red and orange) seem to have lower D_{max}/L ratios than faults whose profiles end with high slip gradients (blue).

3c- Fault lengthening versus slip increase – small-scale features

Additional observations can be made when fault growth is analyzed in greater details. While most faults show an initial phase of rapid lengthening, they do not extend similarly

(supporting online material I). In most cases, the fault looks as lengthening continuously (at the resolution of the experiment), through the lateral propagation of one or both of its tips. In other few cases, the fault lengthens abruptly by connecting to another, initially distinct, fault segment. Generally, that segment initiates just ahead of the expending tip of the main fault, hardly before the connection is made. In more rare cases, the segment initiates at some distance from the expending fault, much before the connection occurs.

Figure 8 shows the details of the incremental growth of two example faults. The faults look like made of small patches that slip differently in both space and time. At any one time-step, the faults slip along their entire length but the slip distribution is highly heterogeneous. At any stage of growth, several patches along the fault slip by large amounts while other zones hardly or do not slip at all (top plots). Moreover, at any stage of growth, there are several, distinct areas along the fault that slip by similar large amounts (middle plots). These large slip zones are not necessarily where the final displacement is the largest, though the zone of final D_{max} is among those slipping most. It is important to note that most of the slip patches do not coincide with any clear segment along the fault trace. Slip increase also varies in time. At any point along a fault, slip increases by variable amounts, commonly alternating from being large to being small (top and middle plots). This results in any slip gap being eventually 'filled' over the entire fault history. The time over which the gap is filled is variable; it is longer in zones where distinct segments have eventually connected. One can note that the incremental slip is generally either much larger (yellow to red, bottom plots) or much lower (pale to dark blue, bottom plots) than the average value that one would infer from scaling the total final slip by the number of slip increments. Finally, the figures also suggest that faults generally grow a bit slower (in term of slip increase) at both the beginning and end of their history (bottom plots).

4- Discussion

Having analyzed before hundreds of natural fault slip profiles, both long-term (Manighetti et al., 2001) and co-seismic (Manighetti et al., 2005), we cannot avoid noting that the analog profiles share many common features with the natural ones. This suggests that the experimental observations are meaningful, and that those common features are inherent properties shared by natural and analogue faults.

4.1- Common features to natural and analog slip profiles

A first feature common to natural and analog slip profiles is their triangular, and commonly asymmetric, envelope shape. Indeed, while it has long been thought that geological faults had elliptical or bell-shaped slip profiles in accordance with the predictions of the elastic crack theory (e.g. Pollard and Segall, 1987; Cowie and Scholz, 1992a-b; Scholz, 2002), a number of recent observations show that faults more commonly exhibit triangular slip distributions (Peacock and Sanderson, 1996; Nicol et al., 1996; Cowie and Shipton, 1998; Cartwright and Mansfield, 1998; Joussineau et al., 2001; Manighetti et al., 2001 for normal faults; Ellis and Dunlap, 1988; Shaw et al., 2002; Davis et al., 2005 for reverse faults; Pachell and Evans, 2002 for strike-slip faults). Besides, although most available fault models assume that maximum displacement is at the fault center (e.g. Pollard and Segall, 1987; Cowie and Scholz, 1992a; Willemse et al., 1996; Cowie and Shipton, 1998; Kim and Sanderson, 2005), natural faults more commonly show asymmetric slip profiles (e.g. Peacock and Sanderson, 1991; Cartwright and Mansfield, 1998; Maerten et al., 1999; Manighetti et al., 2001; Shaw et al., 2002; Pachell and Evans, 2002; Davis et al., 2005). We make similar observations here; most analog faults grow by developing asymmetric, triangular slip profiles, basically made of a long linear section gently tapering to zero at one fault tip while ending through a high slip gradient at the other fault tip. As for natural faults, the long linear sections slant in the direction of fault lengthening (ex: faults e-f, Fig.2). Also as for natural faults, the high slip gradients develop where the fault meets an 'obstacle' (or 'barrier') to its further lengthening (as an example, see the right tip of fault 3ab in figures 1 and 2d). That is commonly a parallel antithetic fault. Thus, as for natural faults, a slip profile remains symmetric as long as the fault has not met any barrier, and starts distorting once one fault tip at least has met an obstacle to its further lengthening. In that case, the zone of maximum slip progressively translates toward the 'arrested' tip, where it may subsequently remain stable for a long time. Yet if the other fault tip also meets a barrier, the zone of D_{max} may shift again laterally. Thus the position of D_{max} may change over the fault lifetime. Furthermore, the zone where slip ends to be largest does not necessarily coincide with the locus of fault initiation, as it has been suggested (e.g. Ellis and Dunlap, 1988). It is important to note that the development of long linear sections in the slip profiles is not in keeping with the elastic crack theory (see Manighetti et al., 2001 for an extended discussion). One way to reconcile these profiles with that theory is to admit that the excess stresses that they produce on the fault plane are diffused off that plane, possibly in the form of distributed damage (Manighetti et al., 2004). We do not have the resolution to verify whether or not such diffuse deformation occurs nearby the linear slants.

A second feature common to natural and analog faults is their bimodal mode of growth; faults are found to grow in two successive phases, an initial period of dominant, rapid lengthening, and a subsequent phase of dominant slip increase with no or little lengthening. Both phases have been observed in natural cases, but the scarcity of available data in respect to the long fault lifetimes (10^5-10^7 yrs) has not allowed describing them in detail (Armijo et al., 1996; Morewood and Roberts, 1999; Contreras et al., 2000; Poulimenos, 2000; Goldsworthy and Jackson, 2001; Meyer et al., 2002; Walsh et al., 2002; Gawthorpe et al., 2003; Childs et al., 2003; Taylor et al., 2004; Bennett et al., 2005; Nicol et al., 2005). The numerical modeling and analog experiment of Cowie and Shipton (1998) and Mansfield and Cartwright (2001) respectively, also suggest the existence of such two phases, but the data are too few to describe them in detail. The initial lengthening phase is brief, hardly more than the third of the fault lifetime (considering the experiment duration as the 'lifetime'), while the lengthening is rapid with most faults reaching more than their half-final length by the end of that initial phase. The lengthening generally occurs through the lateral propagation of the fault tip(s) (see Marchal et al., 1998, for similar observations). We do not have the resolution to determine whether or not the fault tip propagation is a continuous process. Nor do we have the resolution to depict how some faults initiate with a length almost as long as their final one. In any case, such initial long lengths do not result from pre-existing structures being reactivated as suggested or observed in some natural cases (Meyer et al., 2002; Walsh et al., 2002; Nicol et al., 2005; Kim and Sanderson, 2005), nor from the linkage of simultaneously formed major segments, as commonly proposed (e.g., Cowie and Roberts, 2001). While they are lengthening, the faults accumulate some slip. The process is homogeneous overall, such that the D_{max}/L ratio remains constant on each fault and similar for all faults (2 ± 1.10^{-3}). This suggests that faults behave as elastic cracks with constant stress drop during their initial lengthening phase. Following the initial period of rapid lengthening, the faults enter a subsequent phase during which they mainly accumulate vertical slip while hardly or no longer lengthening. Note that while many faults stop lengthening when at least one of their tips has met a barrier, that condition is not required. The phase of dominant slip accumulation is homogeneous as far as it is considered overall. The maximum displacement increases quite regularly on each fault, and in same proportions for all faults. Such a homogeneous vertical growth results in the cumulative slip profiles keeping the same overall shape, -only distorted vertically-, as the faults accumulate more slip. Overall, the phase of dominant slip accumulation lasts longer than that of lengthening, generally about two thirds of the fault life. It makes the faults increasing their D_{max} by 300 % on average (and up to 700%; in respect to

the value of D_{max} at the beginning of the slip accumulation phase). The D_{max}/L ratios increase accordingly during that phase, making the faults not behaving as elastic cracks and not having similar stress drops. By the end of the experiment, most faults still are in a phase of slip accumulation at constant length. We thus have no data to document how the faults go on growing as they accumulate even more strain. In natural cases, it has been found that faults do not accumulate slip over a maximum threshold D_{max}/L ratio averaging 10^{-1} (e.g., Manighetti et al., 2001). This implies that faults must lengthen laterally once they have reached that maximum slip accumulation ratio. This would suggest that faults may resume lengthening by the end of a phase of dominant slip accumulation. The inset of Figure 5a indeed shows a few fault cases that resume lengthening by the end of a slip accumulation phase. It is noteworthy that those few faults have in common to have their tips not being arrested by any clear barrier (see example faults, f6, f11ab or f19 in Fig.1), contrary to the rest of the faults. This suggests that faults pinned at both ends may accumulate more slip without lengthening than unrestricted faults. The same conclusion has been reached for natural cases (Manighetti et al., 2001). Note that, when resuming after a slip accumulation phase, the lengthening occurs through the connection of the main fault with a smaller segment ahead of its tips(s), hence differently than over the initial lengthening period.

A third feature common to analog and natural faults is their capacity of being together homogeneous and heterogeneous; while the fault growth process is clearly homogeneous overall, it is highly irregular in detail. This duality has been suggested for a few geological faults (e.g. Manighetti et al., 2001; Bull et al., 2006), as in a few analog and numerical experiments (Cowie and Shipton, 1998; Mansfield and Cartwright, 2001). The balance between regularity and irregularity roots in the time scale. When the fault growth is considered over a long time span that includes many slip increments, it appears homogeneous; the slip profile maintains the same envelop shape; the slip and length increases are regular overall. In contrast, when the fault growth is considered over time scales that are short in relation to the entire fault history, it appears highly heterogeneous; the slip profile shape exhibits saw-tooth patterns; the slip and length increases are markedly variable in space and time.

4.2- Implications on D_{max}/L 'scaling'

The bimodal growth of the faults causes their maximum displacement and length to change by various proportions over time. As recognized by Mansfield and Cartwright (2001) and Walsh

et al. (2002), those changes produce irregular growth paths in D_{max}-L space, that diverge from the roughly linear relationship that has been derived from available natural D_{max}-L data (D_{max} = k.L with k ≈ 10^{-2}; e.g., Schlische et al., 1996; Manighetti et al., 2001; Davis et al., 2005). The question then arises of whether or not a scaling of the form D_{max} = k.L may be used to prescribe the way natural faults are growing (e.g. Cartwright et al., 1995; Mansfield and Cartwright, 2001). Our experiment suggests that the answer roots in the time scale over which the fault growth process is analyzed. When that process is considered over time scales that are short in relation to the entire fault history, the scaling does not apply and data exhibit a broad range of scatter (Fig.5a). This has been shown to be true in natural cases: on the shortest time scale which is that of individual earthquakes, displacement and length of ruptures are clearly not related by a unique function (Manighetti et al., 2007). By contrast, when the fault growth is considered over a long time span including a large number of slip increments, the linear scaling likely applies, as revealed by the natural data. Thus, for natural faults whose growth history is unknown, the D_{max}-L measurements may be difficult to interpret. Manighetti et al. (2001) have shown that the D_{max}/L ratio of a fault depends on the overall shape of its slip profile: profiles unrestricted at both tips (symmetric triangles) have the lowest ratios reaching at most 2.10^{-2}; those restricted at one tip (asymmetric triangles) have higher ratios with a threshold value of $3\text{-}4.10^{-2}$; those pinned at both tips have the highest values up to 10^{-1}. This suggests that the combined knowledge of a fault slip profile shape and of its corresponding D_{max}/L ratio may indicate the current 'growth mode' of the fault: dominant slip accumulation if the measured ratio is far below the threshold value corresponding to its profile shape; dominant lengthening if that ratio is close to the threshold value. Though more variable, our analog data are in keeping with that inference (supporting online material H).

4.3- Implications on space-time slip and slip rate variability

Determining the rates at which faults slip is a critical issue for these rates indicate the degree of activity of the faults (e.g. Nicol et al., 1997). Numerous studies have thus been conducted in the last 30 years to determine the past and present motion rates on the major active faults worldwide. Most, however, have restricted their analysis to a single slip rate determination at one spot of the fault length (e.g. Wright et al., 2004; Frankel et al., 2007). The underlying assumption is that the slip rate does not vary much along fault strike. Our experiment suggests that this may be incorrect. At any instant of the fault evolution, the displacement varies markedly along the fault length; so thus would the slip rate. Studies providing several slip rate

estimates along a fault actually reach the same conclusion (e.g. Tapponnier et al., 2001; Taylor et al., 2004; Bull et al., 2006). Most studies that report slip rates also implicitly admit that fault rate does not vary much either in time (e.g. Wright et al., 2004). Our experiment shows that this may be incorrect. Figure 8 shows that slip varies widely in time at one given spot of the fault length. Figure 9 is even clearer. In each plot, the black curve is the mean slip rate that one would infer from measuring and dating the total cumulative slip profile. It is thus equivalent to the long-term slip rate profile. The colors dots are the slip rates that one would infer from measuring the slip produced at each step of the growth, with the step duration being known. The black curve clearly results from highly variable slip rates being averaged. This shows that, at any spot of the fault length, the slip rate averaged over a long time span is far different, by an order of magnitude, from the slip rate averaged over a short time span. The incremental rate is particularly low both in the very first and very last stages of the fault growth. The experiment thus demonstrates that the slips and slip rates on faults are markedly variable in both space and time. A similar conclusion has been reached in the rare studies that analyzed the natural fault slip behavior at different space and times scales (e.g. Weldon et al., 2004; Chevalier et al., 2005; Bull et al., 2006). One consequence is that the common assertion that earthquake ruptures showing a similar slip amplitude at one local spot of a fault are characteristic (e.g. Nishenko and Bulland, 1987; Rockwell et al., 2001; Klinger et al., 2003; Haibing et al., 2005) is likely erroneous.

4.4- Proposed scenario of overall fault growth

Figure 10 presents a scenario of overall fault growth that includes the major observations described above. That scenario is only qualitative for modeling the physics of faulting and earthquakes is not the scope of the paper. Also, it only describes the general features of the growth process for a fault that would ideally remain isolated throughout its evolution. Integrating the small-scale complexities of the fault evolution is a further step of work.

In a first phase (Fig.10a), the fault rapidly propagates laterally while accumulating slip in proportion so that, overall, the fault behaves as an elastic crack. At this stage, the lengthening likely occurs continuously. While lengthening, the fault develops a roughly triangular slip profile. As that profile develops, the medium holding the linear slants sustains extended damage, possibly in the form of multiplied micro-cracking (Marder and Fineberg, 1996; Manighetti et al., 2004). Large triangular zones of damage having their apex centered on the

point of fault initiation are requested to maintain a triangular profile (Manighetti et al., 2004). The damage zone accommodates the excess stresses that result from the triangular shape of the slip profile, so that stress on the fault plane remains about constant, compatible with the elastic crack behavior and the self-similarity.

The fault then stops propagating, generally as it starts interacting with nearby faults. Once arrested, the fault continues growing by accumulating more slip (Fig.10b). As it does so, the overall shape of its slip profile is vertically distorted while the stress concentration at its tips increases. The increased amount of stress accommodated within the damage zone likely makes some of the damage cracks growing larger. Some of these cracks may eventually form well-expressed segments ahead of the main fault tips. Since excess stresses are accommodated within the damage zone, the stress on the fault plane still remains about constant.

Once slip, hence stress, accumulation is such that the strength of the damage zone ahead of the fault tips is overcome, we hypothesize that the fault resumes lengthening, likely by connecting to one of the largest damage cracks (Fig.10c). Note that the D_{max}/L ratios of the connecting fault and segment are unlikely to be similar, as commonly assessed (e.g., Cowie and Roberts, 2001). As the fault lengthens, its D_{max}/L ratio drops, while its slip profile remains triangular overall. Since the fault length increases, the damage zone widens. New damage structures are thus created, while previous structures either continue accommodating stress and strain, or become inactive and possibly offset by the lengthening fault.

We suggest that faults basically grow through alternating phases of dominant lengthening and dominant slip accumulation. The initial phase of rapid lengthening that occupies the first third of the fault lifetime is likely different however than any subsequent phase of further lengthening; that initial phase occurs through fault tip propagation, while subsequent lengthening rather occurs through segment connection. Interestingly, the bimodal growth that we describe in Figure 10 is ‘self-driven’ and ‘self-sustaining’: as a fault accumulates some slip, it damages the adjacent medium, particularly at its tips. That damage in turn helps the fault accumulating more slip (without lengthening), for it diffuses the high stresses that would otherwise result on the fault plane, particularly at its tips. As the fault accumulates more slip, stresses increase within the damage zone, so that a few individual fault segments may eventually form ahead of the growing fault. At some level of slip accumulation, the strength of the damage zone is overcome and the fault lengthens by connecting to the segment(s) previously produced ahead of its tips. The process then repeats. It is thus self-driven since the fault itself produces the features that contribute to both its steady growth at constant length

(the damage zone) and its further lengthening (the segments ahead). It is also self-sustaining since, as the fault grows longer, the stresses to be diffused in the damage zone grow higher, making the process unable to stop (in the absence of any local complexity, such as 'external' barriers). One implication is that the segments that eventually connect to form a larger fault, do not initiate randomly nor simultaneously, as commonly assumed (Cowie and Roberts, 2001; Davis et al., 2005; Walsh et al., 2003; Kim and Sanderson, 2005; Nicol et al., 2005). Besides their length is somehow dictated by the 'strength' of the medium (actually, its apparent stiffness) where the fault is growing.

Note that growth in isolation conditions as described above must be seldom. Yet, the encounter of a fault with a barrier does not change the general process. The barrier only increases the strength of the zone ahead of the fault tips, and this may increase the duration of the slip accumulation phase (hence more slip is accumulated), while distorting the slip profile from symmetric to asymmetric.

5- Conclusions

Our laser-equipped analog experiment led to the formation and growth of a dense network of normal faults for which we could measure the slip and length changes at successive short time lapses. This provides a unique opportunity to visualize and quantify the fault growth process and to examine how slip increments follow on a fault to make it grow. The analog faults are found to exhibit a number of features similar to those observed on geological faults. This suggests that these features may be intrinsic properties of faults, which thus should be reproduced by fault models. This furthermore suggests that the experiment is meaningful, with its results likely to apply to faults of any slip mode. The quasi-continuous observation of the fault growth that we perform allows us to examine these properties with far more detail than what is possible on natural faults. The major properties that we have identified are the following:

- Slip distributions have linear sections almost as long as the entire faults, and those sections generally persist during the fault evolution. This observation is not in keeping with the elastic crack theory. It suggests that extended damage of the medium is likely to result from the growth of a fault.
- Faults start growing in two successive phases: an initial, short (first third of the fault lifetime) period dominated by rapid lengthening, followed by a subsequent, longer (last two thirds of the fault lifetime) phase of mainly slip increase at roughly constant length.

- Faults are likely to go on growing through the alternation of phases of dominant lengthening and phases of dominant slip accumulation. Additional data are however necessary to confirm this hypothesis. Such bimodal growth is likely to be 'self-driven' and 'self-sustaining'.
- Faults grow overall homogeneously even though the individual slip events are characterized by large slip and stress heterogeneities. This suggests that there is a feedback between stress heterogeneities and slip development. The consequence of this is that the long-term faulting process is primarily insensitive to the short-term heterogeneities that are rapidly smoothed or redistributed.

One implication of this duality between heterogeneous and homogeneous behavior is that the short- and long-term slips and slip rates on natural faults are likely to be markedly different. Successive slip events are likely to also significantly differ in both slip amplitude and distribution. Together these results call for great caution when interpreting the available slip data on faults and ruptures, particularly when doing so in terms of 'characteristic earthquakes', as commonly done.

Acknowledgments:

This work has been funded by the INSU-CNRS Dyeti program, and by the French ANR (project QUAKonSCARPS, n° ANR-06-CATT-008-01 and ANR-06-CATT-008-03). We thank M. Campillo, F. Cotton, Y. Delaby, and Y. Gaudemer for fruitful discussions. We are also grateful to two anonymous reviewers whose thorough and constructive comments helped improve the manuscript.

REFERENCES

Ackermann, R.V., Schlische, R.W., Withjack, M.O., 2001. The geometric and statistical evolution of normal fault systems: an experimental study of the effects of mechanical layer thickness on scaling laws. J. Struct. Geol. 23, 1803-1819.

Armijo, R., Meyer, B., King, G., Rigo, A., Papanastassiou, D., 1996. Quaternary evolution of the Corinth rift and its implications for the late Cenozoic evolution of the Aegean. Geophys. J. Int. 126(1), 11–53.

Bellahsen, N., Daniel, J.M., Bollinger, L., Burov, E., 2003. Influence of viscous layers on the growth of normal faults: insights from experimental and numerical models. J. Struct. Geol. 25, 1471–1485.

Bellahsen, N., Daniel, J.M., 2005. Fault reactivation control on normal fault growth: an experimental study. J. Struct. Geol. 27, 769–780.

Bennett E., Youngson, J. H., Jackson, J., Norris, R., Raisbeck, G., Yiou, F., Fielding, E., 2005. Growth of South Rough ridge, Central Otago, New Zealand: using in situ cosmogenic isotopes and geomorphology to study an active, blind reverse fault. Journal of Geophysical Research. 110(B02404), doi:10.1029/2004JB003184.

Buiter, S., Schreurs, G., editors, 2006. Analogue and Numerical Modelling of Crustal-Scale Processes. 253. Geological Society, London, Special Publications.

Bull, J., Barnes, P., Lamarche, G., Sanderson, D., Cowie, P., Taylor, S., Dix, J., 2006. High-resolution record of displacement accumulation on an active normal fault system: implications for models of slip accumulation during repeated earthquakes. J. Struct. Geol. 28(7), 1146–1166.

Bürgmann, R., Pollard, D., Martel, S., 1994. Slip distributions on faults: effects of stress gradients, inelastic deformation, heterogeneous host-rock stiffness, and fault interaction. J. Struct. Geol. 16(12), 1675–1690.

Bürgmann, R., Rosen, P., Fielding, E., 2000. Synthetic aperture radar interferometry to measure Earth's surface topography and its deformation. Annual Review of Earth and Planet. Sci. 28, 169–209.

Cartwright, J., Trudgill, B., Mansfield, C., 1995. Fault growth by segment linkage: an explanation for scatter in maximum displacement and trace length data from the Canyonlands gradens of SE Utah. J. Struct. Geol. 17(9), 1319–1326.

Cartwright, J., Mansfield, C., 1998. Lateral displacement variations and lateral tip geometry of normal faults in the Canyonlands National park, Utah. J. Struct. Geol. 20(1), 3–19.

Chevalier, M.L., Ryerson, F.J., Tapponnier, P., Finkel, R.C., Van der Woerd, J., Haibing, L., Qing, L., 2005. Slip-rate measurements on the Karakorum fault may imply secular variations in fault motion. Science. 307, 411–414.

Childs, C., Nicol, A., Walsh, J., Watterson, J., 2003. The growth and propagation of synsedimentary faults. J. Struct. Geol. 25, 633–648.

Contreras, J., Anders, M., Scholz, C., 2000. Growth of a normal fault system: observations from the lake Malawi basin of the East African rift. J. Struct. Geol. 22, 159–168.

Cowie, P., Scholz, C., 1992a. Physical explanation for the displacement-length relationship of faults using a post-yield fracture mechanics model. J. Struct. Geol. 14(10), 1133–1148.

Cowie, P., Scholz, C., 1992b. Displacement-length scaling relationship for faults: data synthesis and discussion. J. Struct. Geol. 14(10), 1149–1156.

Cowie, P., Shipton, Z., 1998. Fault tip displacement gradients and process zone dimensions. J. Struct. Geol. 20(8), 983–997.

Cowie, P., 1998. A healing-reloading feedback control on the growth rate of seimogenic faults. J. Struct. Geol. 20(8), 1075–1087.

Cowie, P., Roberts, G., 2001. Constraining slip rates and spacing for active normal faults. J. Struct. Geol. 23, 1901–1915.

Daeron M., Klinger, Y., Tapponnier, P., Elias, A., Jacques, E., Sursock, A., 2005. Sources of the large a.d. 1202 and 1759 near east earthquakes. Geology. 33(7), 529–532.

Davis, K., Burbank, D., Fisher, D., Wallace, S., Nobes, D., 2005. Thrust-fault growth and segment linkage in the active Ostler fault zone, New Zealand. J. Struct. Geol. 27, 1528–1546.

Davy, P., Cobbold, P., 1991. Experiments on shortening of a 4-layer model of the continental lithosphere. Tectonophysics. 188(1-2), 1–25.

Davy, P., Hansen, A., Bonnet, E., Zhang, S.Z., 1995. Localization and fault growth in layered brittle-ductile systems: implications for deformations of the continental lithosphere. J. Geophys. Res. 100(B4), 6281–6294.

Ellis, M., Dunlap, W., 1988. Displacement variation along thrust faults: implications for the development of large faults. J. Struct. Geol. 10(2), 183–192.

Faugeres, E., Brun, J.P., 1984. Modélisation expérimentale de la distension continentale. Comptes rendus de l'Académie des Sciences de Paris. 299, 365-370.

Frankel K.L., Brantley, K.S., Dolan, J.F., Finkel, R.C., Klinger, R.E., Knott, J.R., Machette, M.N., Owen, L.A., Phillips, F.M., Slate, J.L., Wernicke, B.P., 2007. Cosmogenic 10Be and 36Cl geochronology of offset alluvial fans along the northern Death Valley fault zone: implications for transient strain in the Eastern California Shear Zone. J. Geophys. Res. 112 (B06407), doi:10.1029/2006JB004350.

Gawthorpe, R., Jackson, C.L., Young, M., Sharp, I., Moustafa, A., Leppard, C., 2003. Normal fault growth, displacement localisation and the evolution of normal fault populations: the Hammam Faraun fault block, Suez rift, Egypt. J. Struct. Geol. 25, 883–895.

Goldsworthy, M., Jackson, J., 2001. Migration of activity within normal fault systems: examples from the quaternary of mainland Greece. J. Struct. Geol. 23(2-3), 489-506.

Graveleau, F., Dominguez, S., 2008. Analogue modelling of the interaction between tectonics, erosion and sedimentation in foreland thrust belts. C. R. Geosciences. 340, 324-333.

Haibing, L., Van der Woerd, J., Tapponnier, P., Klinger, Y., Xuexiang, Q., Jingsui, Y., Yintang, Z., 2005. Slip rate on the Kunlun fault at Hongshui Gou, and recurrence time of great events comparable to the 14/11/2001, Mw 7.9 Kokoxili earthquake. Earth Planet. Sci. Lett. 237, 285–299.

Horsfield, W.T., 1977. An experimental approach to basement-controlled faulting. Geologie en Mijnbouw. 56(4), 363-370.

Hubbert, M.K., 1937. Theory of scale models as applied to the study of geologic structures. Geol. Soc. Am. Bull. 48(10), 1459–1519.

de Joussineau, G., Bouissou, S., Petit, J.P., Barquins, M., 2001. Experimental analysis of slip distribution along a fault segment under stick-slip and stable sliding conditions. Tectonophysics. 337, 85–98.

Kim, Y., Sanderson, D., 2005. The relationship between displacement and length of faults. Earth-Science Reviews. 68, 317–334.

Klinger, Y., Sieh, K., Altunel, E., Akoglu, A., Barka, A., Dawson, T., Gonzalez, T., Meltzner, A., Rockwell, T., 2003. Paleoseismic evidence of characteristic slip on the western segment of the North Anatolian fault, Turkey. Bull. Seism. Soc. Am. 93(6), 2317–2332.

Lallemand, S., Malavieille, J., 1992. Coulomb theory applied to accretionary and non-accretionary wedges. Eos, Trans., Am. Geophys. Union. 73(14), 7–23.

Lohrman J., Kukowski, N., Adam, J., Oncken, O., 2003. The impact of analogue material properties on the geometry, kinematics and dynamics of convergent sand wedges. J. Struct. Geol., 25, 1691–1711.

Maerten, L., Willemse, E., Pollard, D., Rawnsley, K., 1999. Slip distributions on intersecting normal faults. J. Struct. Geol. 21, 259–271.
Manighetti, I., King, G., Gaudemer, Y., Scholz, C., Doubre, C., 2001. Slip accumulation and lateral propagation of active normal faults in Afar. J. Geophys. Res. 106(B7), 13667–13696.
Manighetti, I., King, G., Sammis, C., 2004. The role of off-fault damage in the evolution of normal faults. Earth Planet. Sci. Lett. 217, 399–408.
Manighetti, I., Campillo, M., Sammis, C., Mai, P., King, G., 2005. Evidence for self-similar, triangular slip distributions on earthquakes: implications for earthquake and fault mechanics. J. Geophys. Res. 110(B05302), doi:10.1029/2004JB003174.
Manighetti, I., Campillo, M., Bouley, S., Cotton, F., 2007. Earthquake scaling, fault segmentation and structural maturity. Earth Planet. Sci. Lett. 253, 429-438.
Mansfield, C., Cartwright, J., 2001. Fault growth by linkage: observations and implications from analogue models. J. Struct. Geol. 23, 745–763.
Marchal, D., Guiraud, M., Rives, T., Van der Driessche, J., 1998. Space and time propagation processes of normal faults. In: Jones, G., Fisher, Q.P. & Knipe, R.J. (eds) Faulting, Fault Sealing and Fluid Flow in Hydrocarbon Reservoirs, Geol. Soc., London, Special Publications. 147, 51–70.
Marchal, D., Guiraud, M., Rives, T., 2003. Geometric and morphologic evolution of normal fault planes and traces from 2D to 4D data. J. Struct. Geol. 25, 135–158.
Marder M., Fineberg, J., 1996. How things break. Phys. Today. 49, 24.
Marrett, R., Allmendinger, R.W., 1991. Estimates of strain due to brittle faulting: sampling of fault populations. J. Struct. Geol. 13(6), 735–738.
Meyer, V., Nicol, A., Childs, C., Walsh, J., Watterson, J., 2002. Progressive localisation of strain during the evolution of a normal fault population. J. Struct. Geol. 24, 1215–1231.
Morewood, N., Roberts, G., 1999. Lateral propagation of the surface trace of the south Alkyonides normal fault segment, central Greece: its impact on models of fault growth and displacement-length relationships. J. Struct. Geol. 21, 635–652.
Nicol, A., Watterson, J., Walsh, J., Childs, C., 1996. The shapes, major axis orientations and displacement patterns of fault surfaces. J. Struct. Geol. 18(2-3), 235–248.
Nicol A., Walsh, J.J., Watterson, J., Underhill, J.R., 1997. Displacement rates of normal faults. Nature. 390, 157-159.
Nicol, A., Walsh, J., Berryman, K., Nodder, S., 2005 Growth of a normal fault by accumulation of slip over millions of years. Journal of Structural Geology. 27, 327–342.
Nishenko, S.P., Bulland, R., 1987. A generic recurrence interval distribution for earthquake forecasting. Bull. Seism. Soc. Am. 77, 1382-1399.
Pachell, M.A., Evans, J., 2002. Growth, linkage, and termination processes of a 10-km-long strike-slip fault in jointed granite: the Gemini fault zone, Sierra Nevada, California. J. Struct. Geol. 24, 1903–1924.
Palumbo, L., Benedetti, L., Bourles, D., Cinque, A., Finkel, R., 2004. Slip history of the Magnola fault (Apennines, Central Italy) from 36Cl surface exposure dating: evidence for strong earthquakes over the Holocene. Earth Planet. Sci. Lett. 225, 163–176.
Peacock, D., Sanderson, D., 1991. Displacements, segment linkage and relay ramps in normal fault zones. J. Struct. Geol. 13(6), 721–733.
Peacock, D., Sanderson, D., 1996. Effects of propagation rate on displacement variations along faults. J. Struct. Geol. 18(2-3), 311–320.
Pollard, D.D., Segall, P., 1987. Theoretical displacements and stresses near fractures in rock: with applications to faults, joints, veins, dikes, and solution surfaces. In: Fracture Mechanics of Rocks (ed. by Atkinson, B.K.). Acad. Press Geology Series, London.

Poulimenos, G., 2000. Scaling properties of normal fault populations in the Western Corinth graben, Greece: implications for fault growth in large strain settings. J. Struct. Geol. 22, 307–322.

Rice, J.R., Ben-Zion, Y., 1996. Slip complexity in earthquake fault models. Proc. Nat. Acad. Sci. USA. 93, 3811-3818.

Rockwell, T., Barka, A., Dawson, T., Akyuz, S., Thorup, K., 2001. Paleoseismology of the Gazikoy-Saros segment of the North Anatolia fault, northwestern Turkey: comparison of the historical and paleoseismic records, implications of regional seismic hazard, and models of earthquake recurrence. J. Seismology. 5(3), 433–448.

Schlische, R., Young, S., Ackermann, R., Gupta, A., 1996. Geometry and scaling relations of a population of very small rift-related normal faults. Geology. 24(8), 683–686.

Scholz, C., 2002. The Mechanics of Earthquakes and Faulting. Cambridge University Press.

Schreurs, G., Hänni, R., Vock, P., 2002. The influence of brittle-viscous multilayers on faulting during rifting: an analogue modelling approach. In: Schellart, W.P. and Passchier, C., Analogue modelling of large-scale tectonic processes. J. Virt. Expl. 6, 89–97.

Segall, P., Pollard, D., 1980. Mechanics of discontinuous faults. J. Geophys. Res. 85(B8), 4337–4350.

Shaw J.H., Plesch, A., Dolan, J.F., Pratt, T.L., Fiore, P., 2002. Puente Hills blind-thrust system, Los Angeles, California. Bull. Seism. Soc. Am. 92, 2946-2960.

Shimazaki, K., Nakata, T., 1980. Time predictable recurrence model for large earthquakes. Geophys. Res. Lett. 7, 279-282.

Tapponnier, P., Ryerson, F.J., Van der Woerd, J., Mériaux, A.S., Lasserre, C., 2001. Long-term slip rates and characteristic slip: keys to active fault behaviour and earthquake hazard. C. R. Acad. Sci. Paris. 333, 483-494.

Taylor, S., Bull, J., Lamarche, G., Barnes, P., 2004. Normal fault growth and linkage in the Whakatane graben, New Zealand, during the last 1.3 myr. J. Geophys. Res. 109, doi:10.1029/2003JB002412.

Tse, S.T., Rice, J.R., 1986. Crustal earthquake instability in relation to the depth variation of frictional slip properties. J. Geophys. Res. 91, 9452-9472.

Walsh, J., Watterson, J., 1987. Distributions of cumulative displacement and seismic slip on a normal fault surface. J. Struct. Geol. 9(8), 1039–1046.

Walsh, J., Watterson, J., 1988. Analysis of the relationship between displacements and dimensions of faults. J. Struct. Geol. 10(3), 239–247.

Walsh, J., Nicol, A., Childs, C., 2002. An alternative model for the growth of faults. J. Struct. Geol. 24, 1669–1675.

Walsh J.J., Bailey, W.R., Childs, C., Nicol, A., Bonson, C.G., 2003. Formation of segmented normal faults: a 3D perspective. J. Struct. Geol. 25, 1251-1262.

Weldon, R., Scharer, K., Fumal, T., Biasi, G., 2004. Wrightwood and the earthquake cycle : What a long reccurence record tells us about how faults work. GSA Today. 14(9), 4–10.

Willemse, E., Pollard, D., Aydin, A., 1996. Three-dimensional analyses of slip distributions on normal fault arrays with consequences for fault scaling. J. Struct. Geol. 18(2/3), 295–309.

Wright T.J., Parsons, B., England, P.C., Fielding, E.J., 2004. InSAR observations of low slip rates on the major faults of Western Tibet. Science. 305, 236-239.

Figure caption:

Figure 1: Map view of the analog model at the end of the experiment. The frame is the zone under study. Analyzed faults are circled in black, with their names indicated. Synthetic and antithetic faults appear in different tones due to shading.

Figure 2: Slip-length profiles on six example faults (location in Fig.1). Naming a fault 'ab' for instance means that the fault, that contains two segments a and b, is considered as a whole. The color scale indicates the successive time steps, in percentage of extension. Stages 1 and 2 do not appear for no surface escarpment was formed at these stages.

Figure 3: Variation over time of the along-strike position of the maximum displacement D_{max}. Each point represents the position of D_{max} at each stage of the fault growth, hence is (X_{Dmax}/X_i), with X_i the length of the fault at stage i, and X=0 taken at the left tips of the faults. For clarity reasons, only the largest faults are represented.

Figure 4: Fault length increase as a function of time. On the X axis, time (T_i) is normalized by the total duration of the fault growth (T_f). On the Y axis, the length (L_i) is normalized by the final total length of the faults (L_f). See discussion in text.

Figure 5: a) Evolution of maximum displacement with fault lengthening. Faults possibly sustaining alternating phases of dominant lengthening and of dominant slip accumulation are highlighted in inset. b) Evolution of maximum displacement with time. See discussion in text.

Figure 6: Increase in vertical slip as a function of time. On the X axis, time (T_i) is normalized by the total duration of the fault growth (T_f). On the Y axis, the maximum slip ($D_{max}i$) is normalized by the final total maximum displacement on the faults ($D_{max}f$).

Figure 7: Variation of the D_{max}/L ratio with fault lengthening. a) Faults whose growth starts by an observable, rapid lengthening phase. That occurs at roughly constant D_{max}/L ratio (grey horizontal bar). b) Faults whose initial lengthening phase is too rapid to be observed (it occurred at less than 5% of extension); those faults thus appear as mainly growing by increasing their slip. See discussion in text.

Figure 8: Space-time slip variability during fault growth. For both fault examples, top plots present the successive slip increments in absolute amplitude (mm); middle plots present the slip increments each normalized by its maximum slip value ($D_{max}i$); bottom plots present the slip increments each normalized by the average value of the maximum slip ($D_{max}f/N$, with $D_{max}f$ the maximum slip value at the end of the experiment and N the number of slip increments).

Figure 9: Comparison of 'long-term' and 'short-term' slip rates. For both fault examples, the black curve is the long-term slip rate profile that one would infer from dividing the final cumulative slip profile by the total number of growth time steps. Conversely, the color crosses represent the short-term slip rates that one would infer from dividing each incremental slip value by one single time lapse. Colors indicate, as before, the succession in time.

Figure 10: A qualitative scenario of fault growth compatible with the observations. The scenario is drawn for an ideal, isolated fault, thus having a triangular, symmetric slip profile. Top plots present the slip distribution on the growing fault. Middle plots present the fault in map view. Bottom plots presents the stress distribution resulting in the 'faulted volume' (fault plane + damage zone). The dotted grey lines remind the previous stages. See the text for more details.

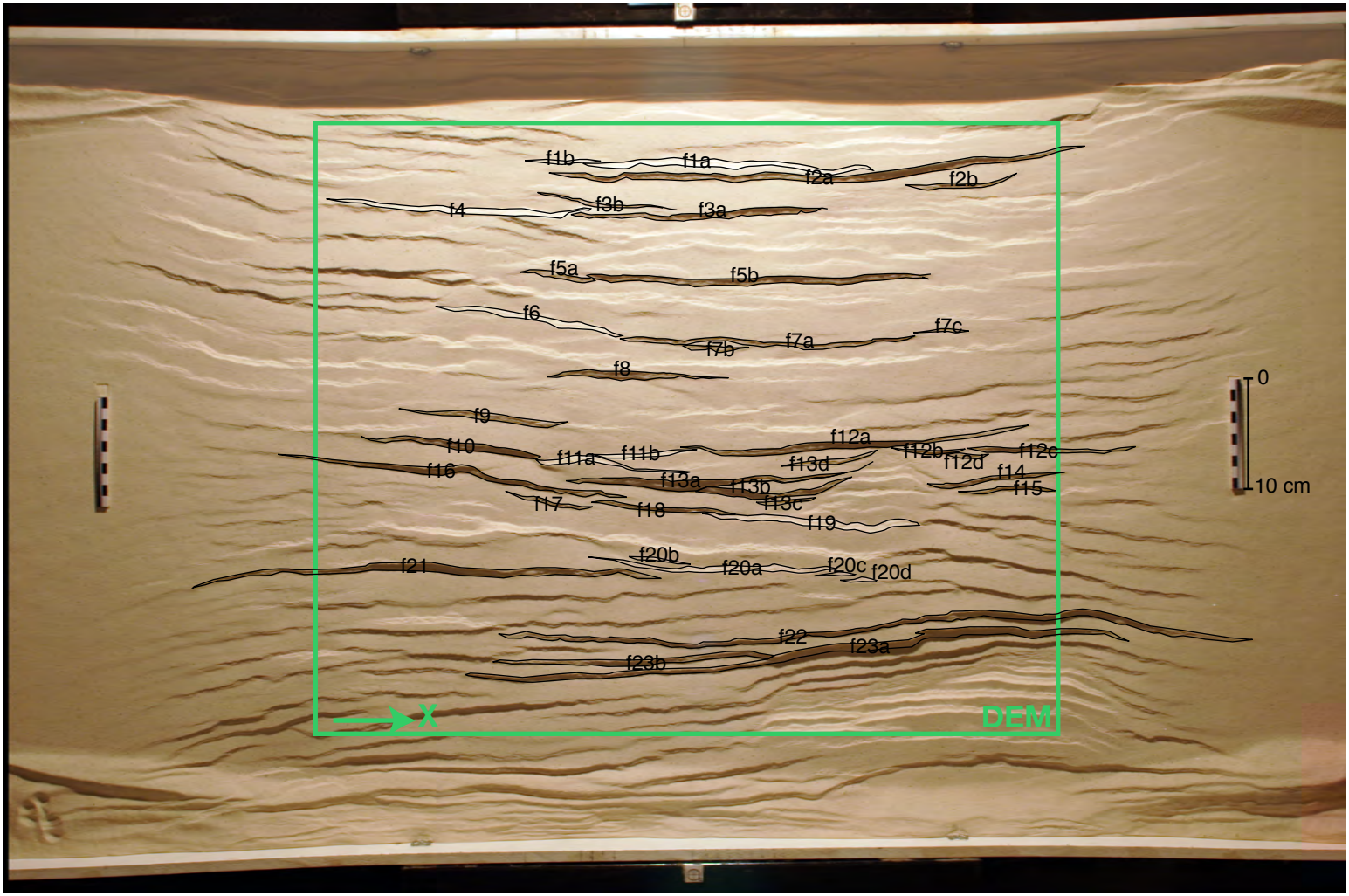

FIGURE 1 - Schlagenhauf et al.

FIGURE 2 - Schlagenhauf et al.

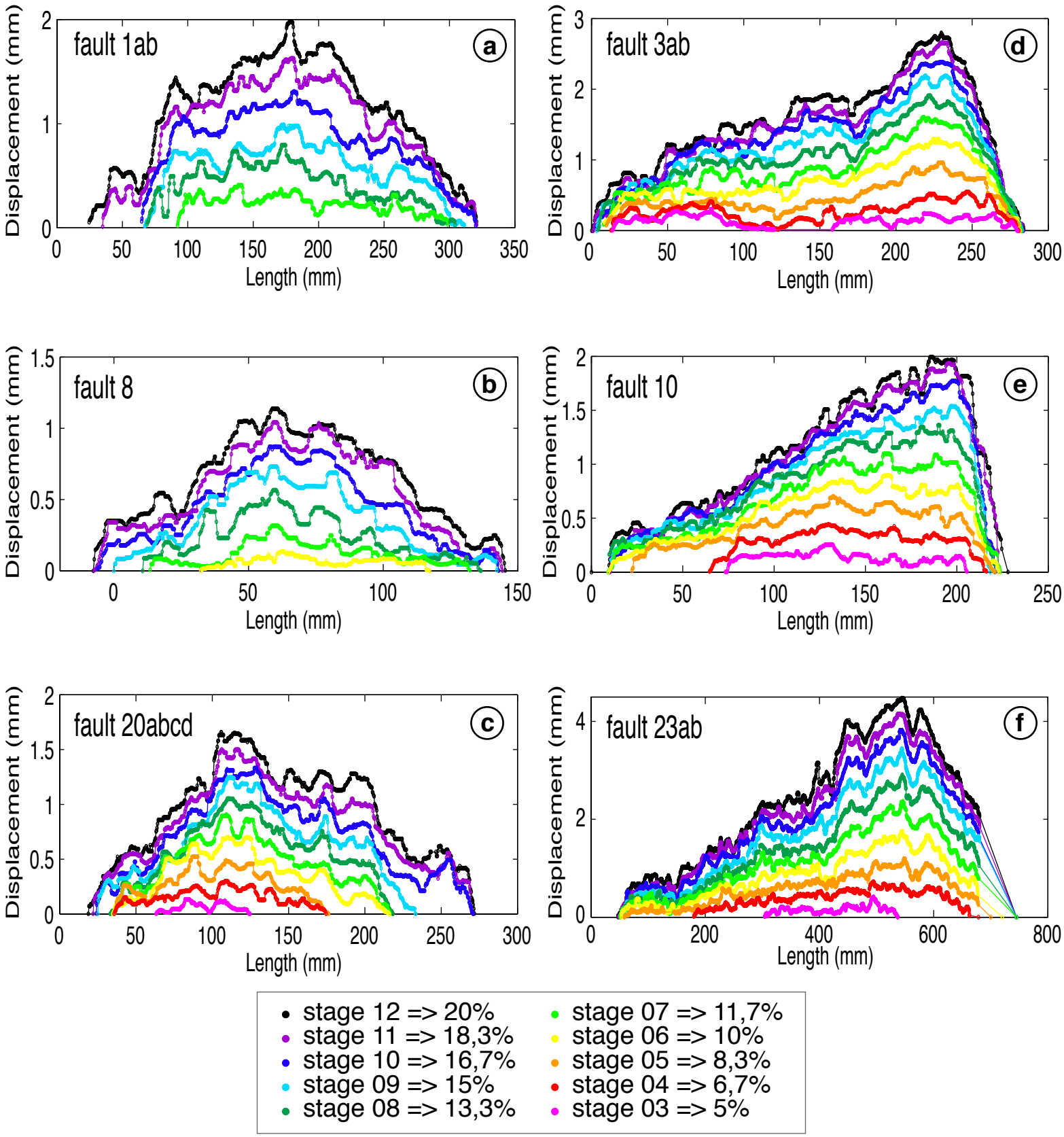

FIGURE 3 - Schlagenhauf et al.

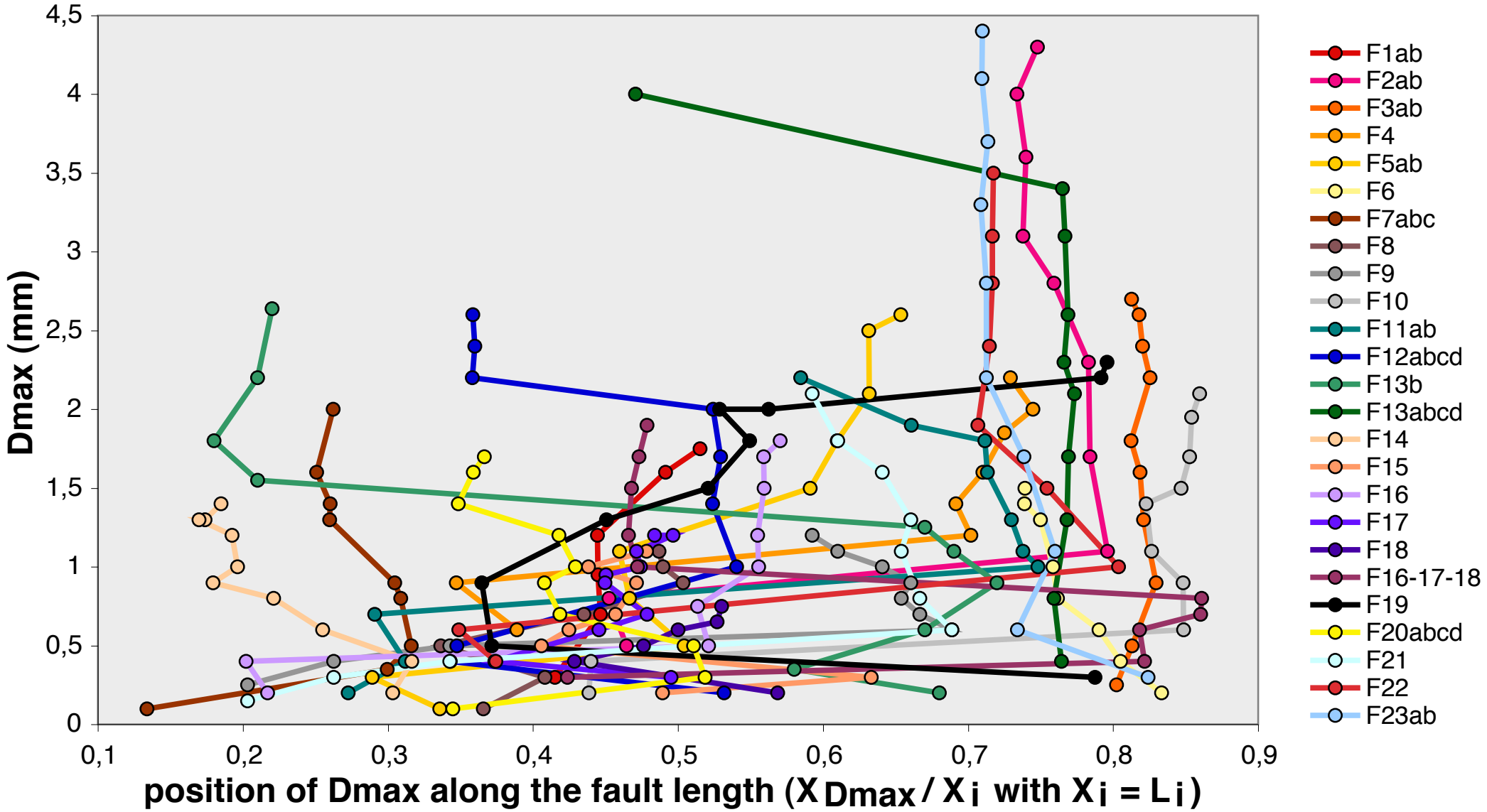

FIGURE 4 - Schlagenhauf et al.

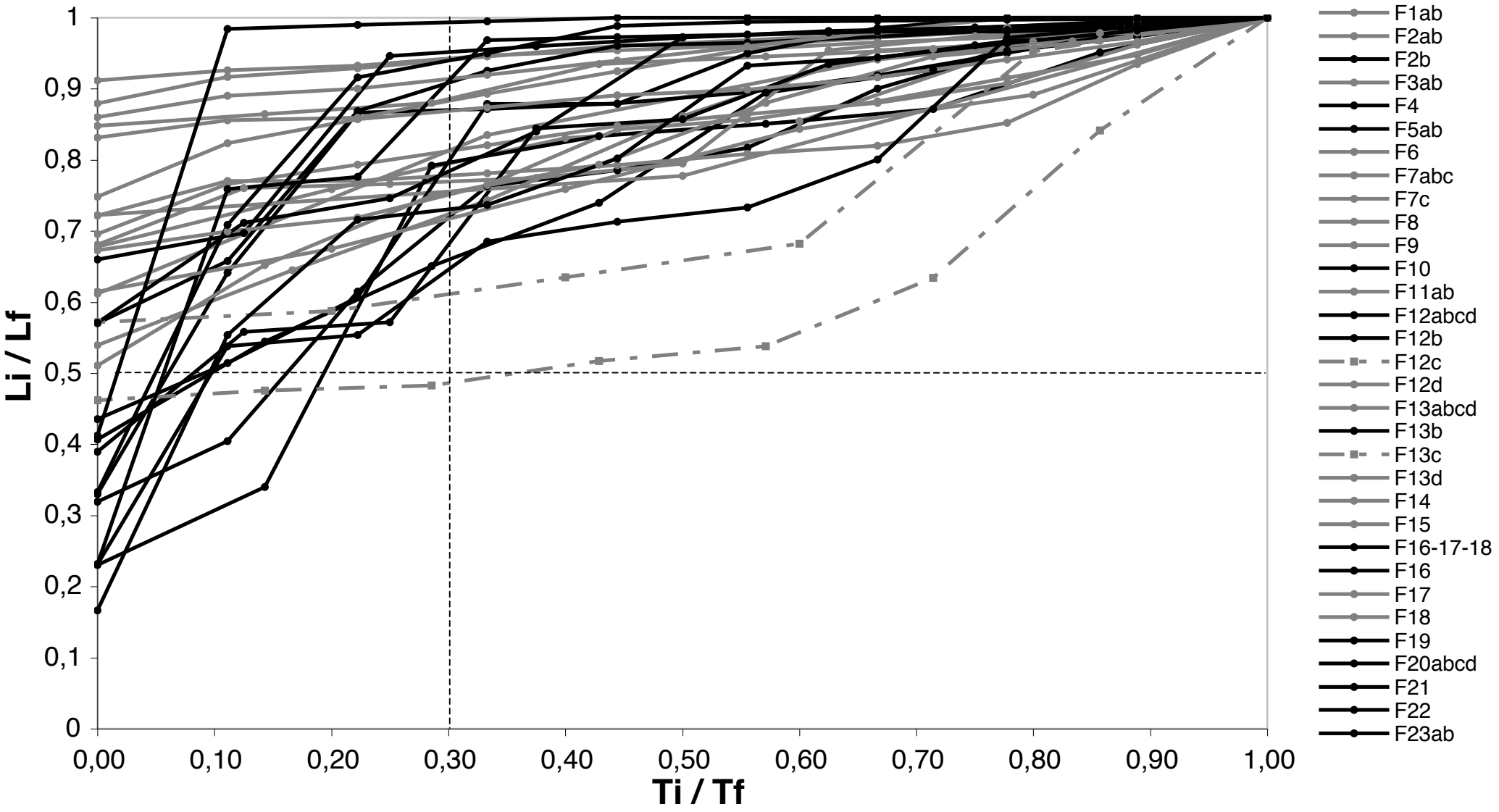

FIGURE 5a - Schlagenhauf et al.

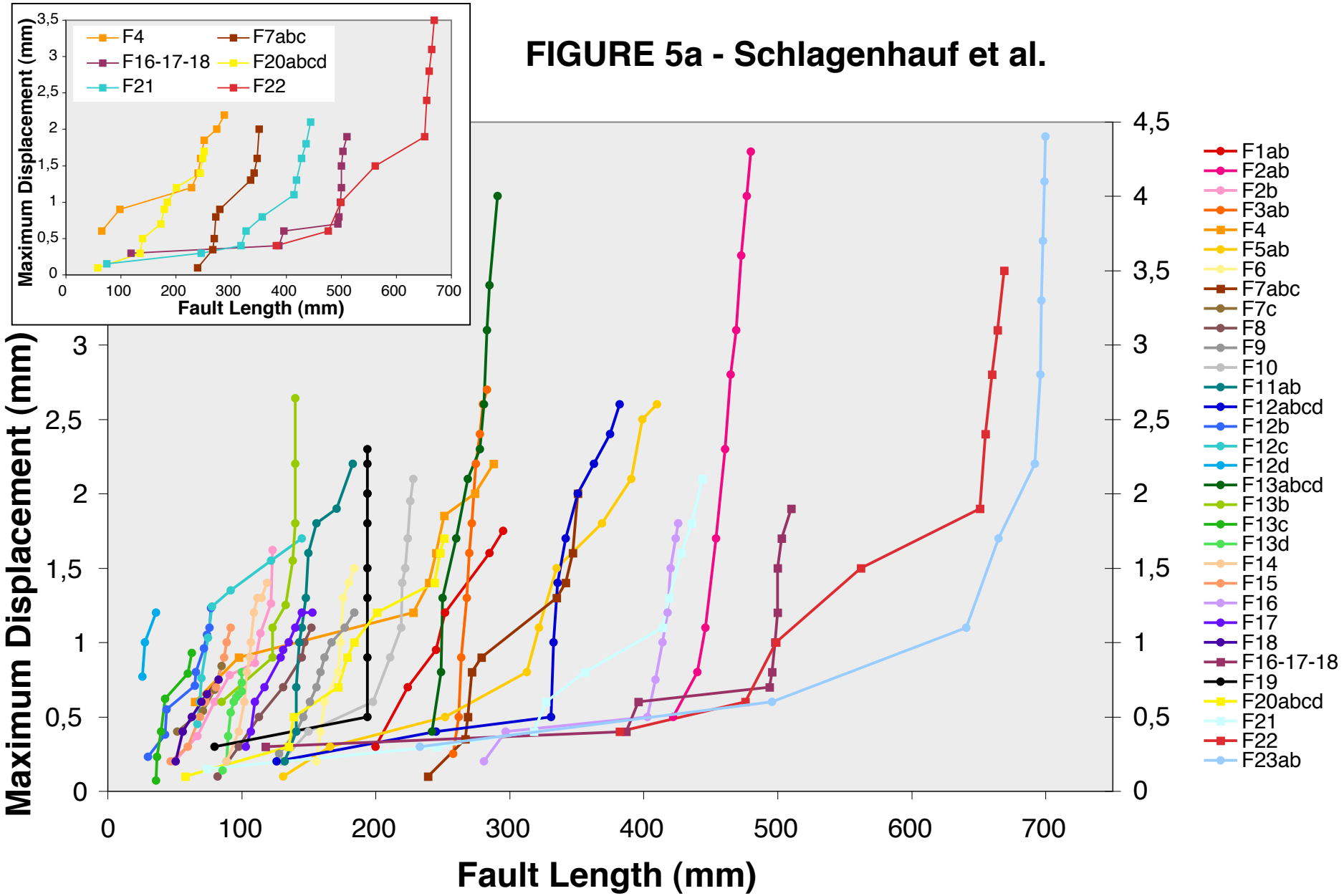

FIGURE 5b - Schlagenhauf et al.

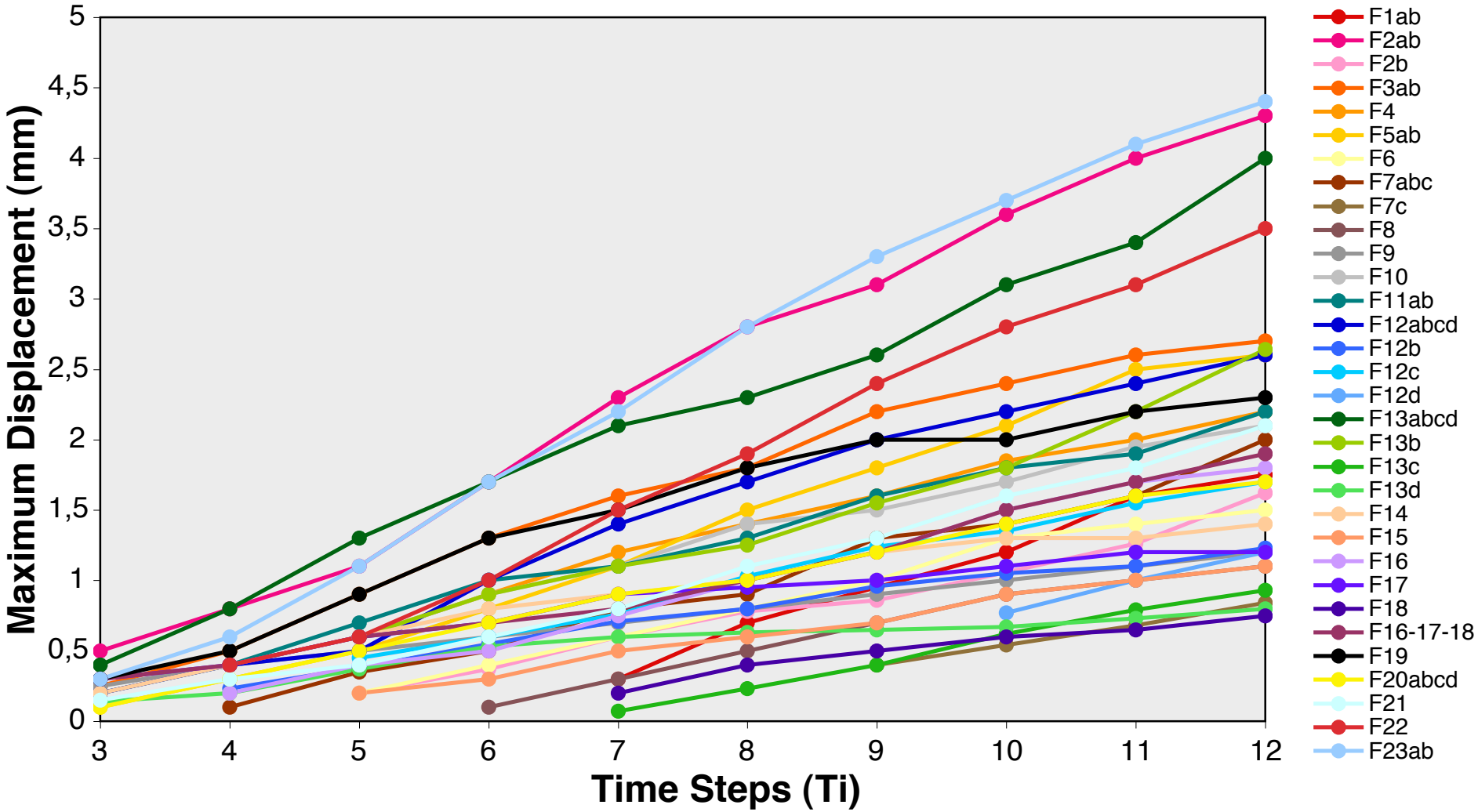

FIGURE 6 - Schlagenhauf et al.

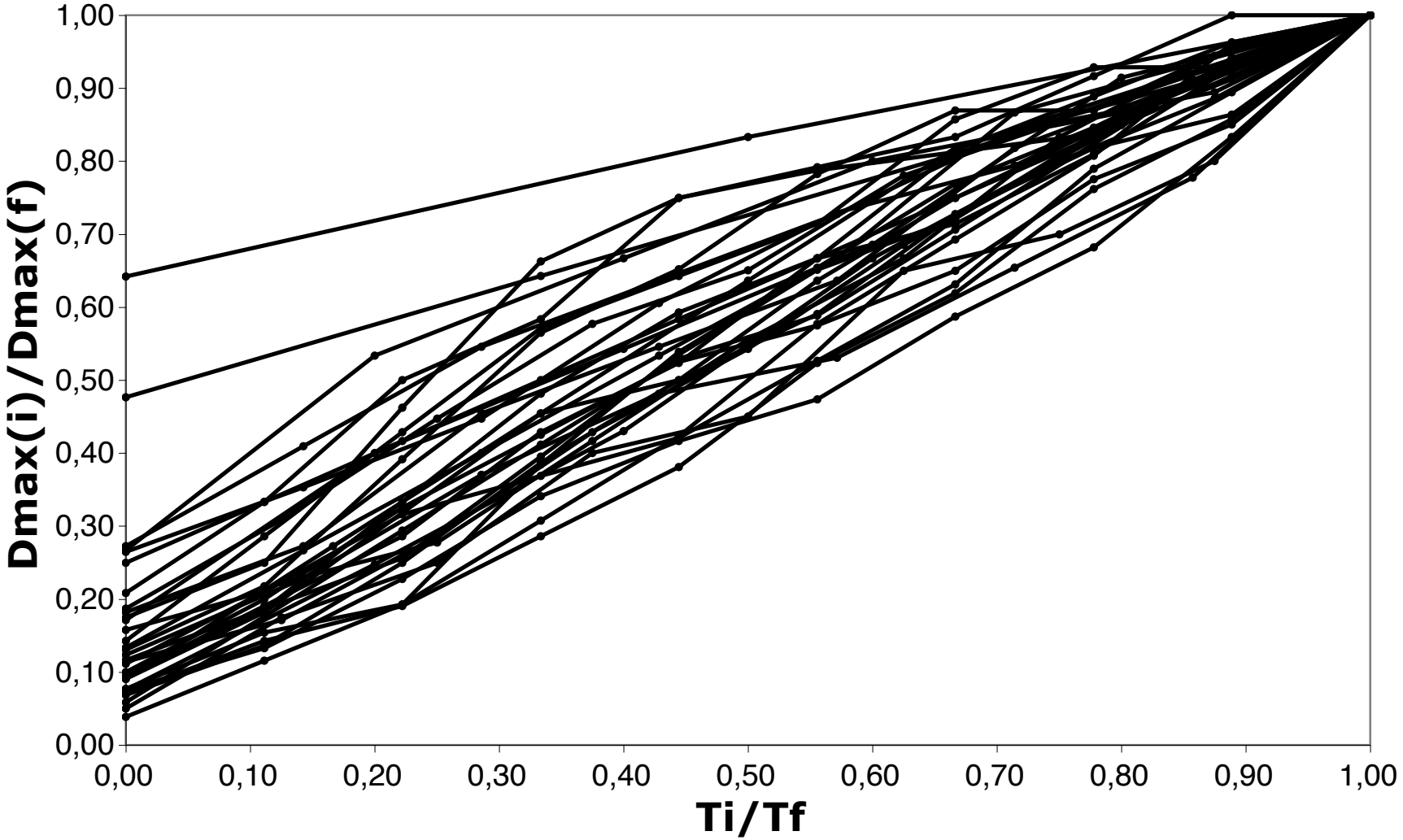

FIGURE 7a - Schlagenhauf et al.

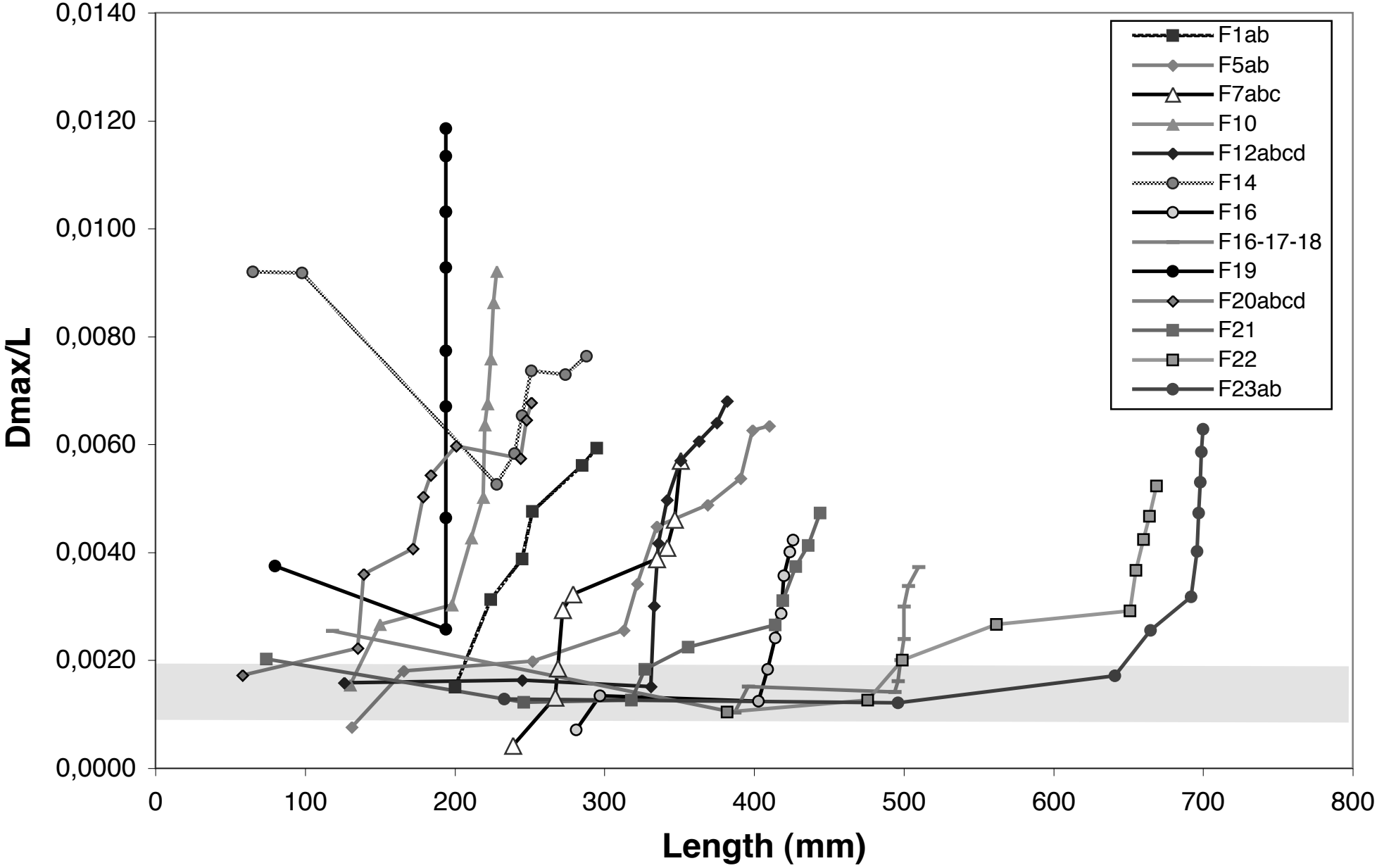

FIGURE 7b - Schlagenhauf et al.

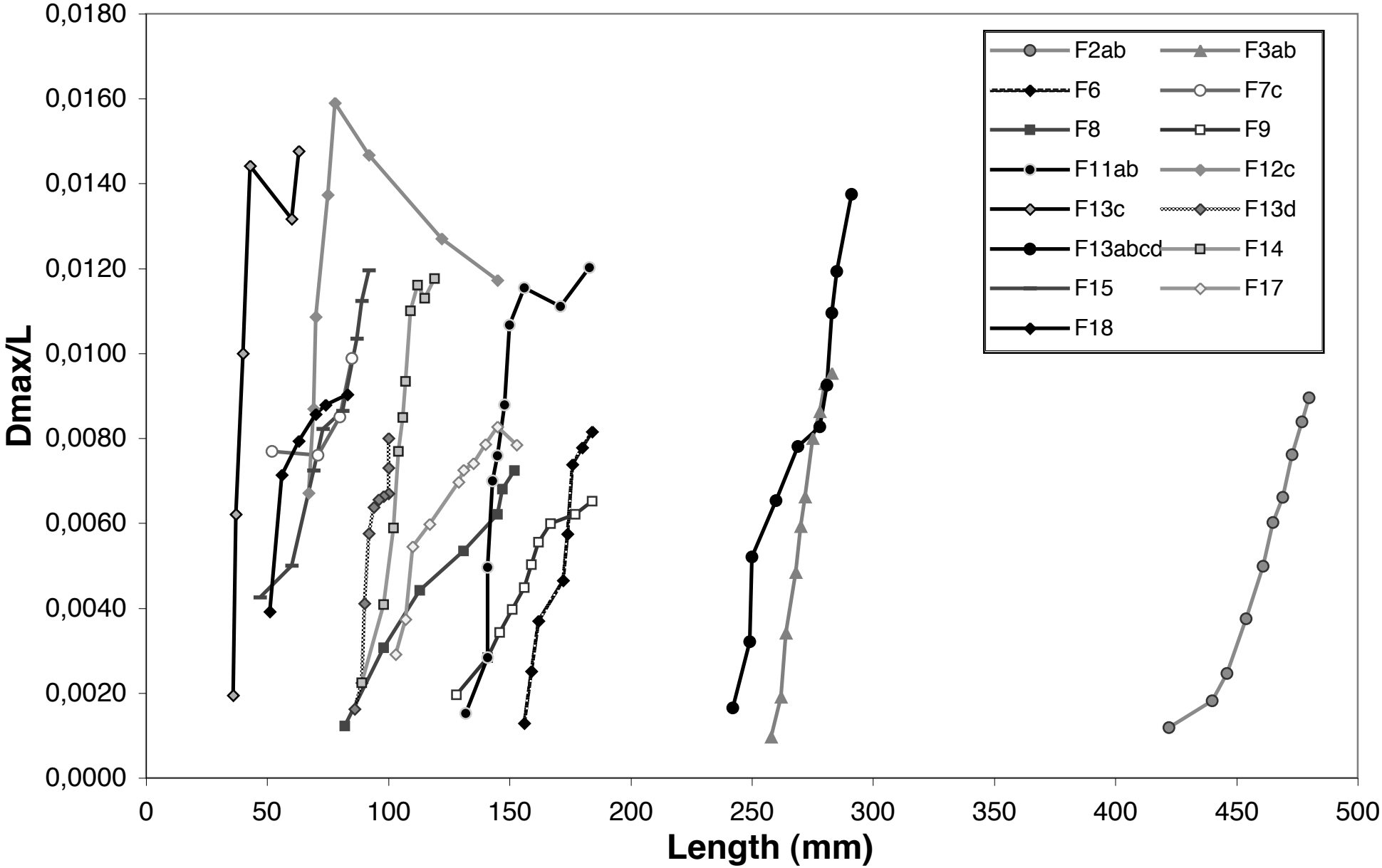

FIGURE 8 - Schlagenhauf et al.

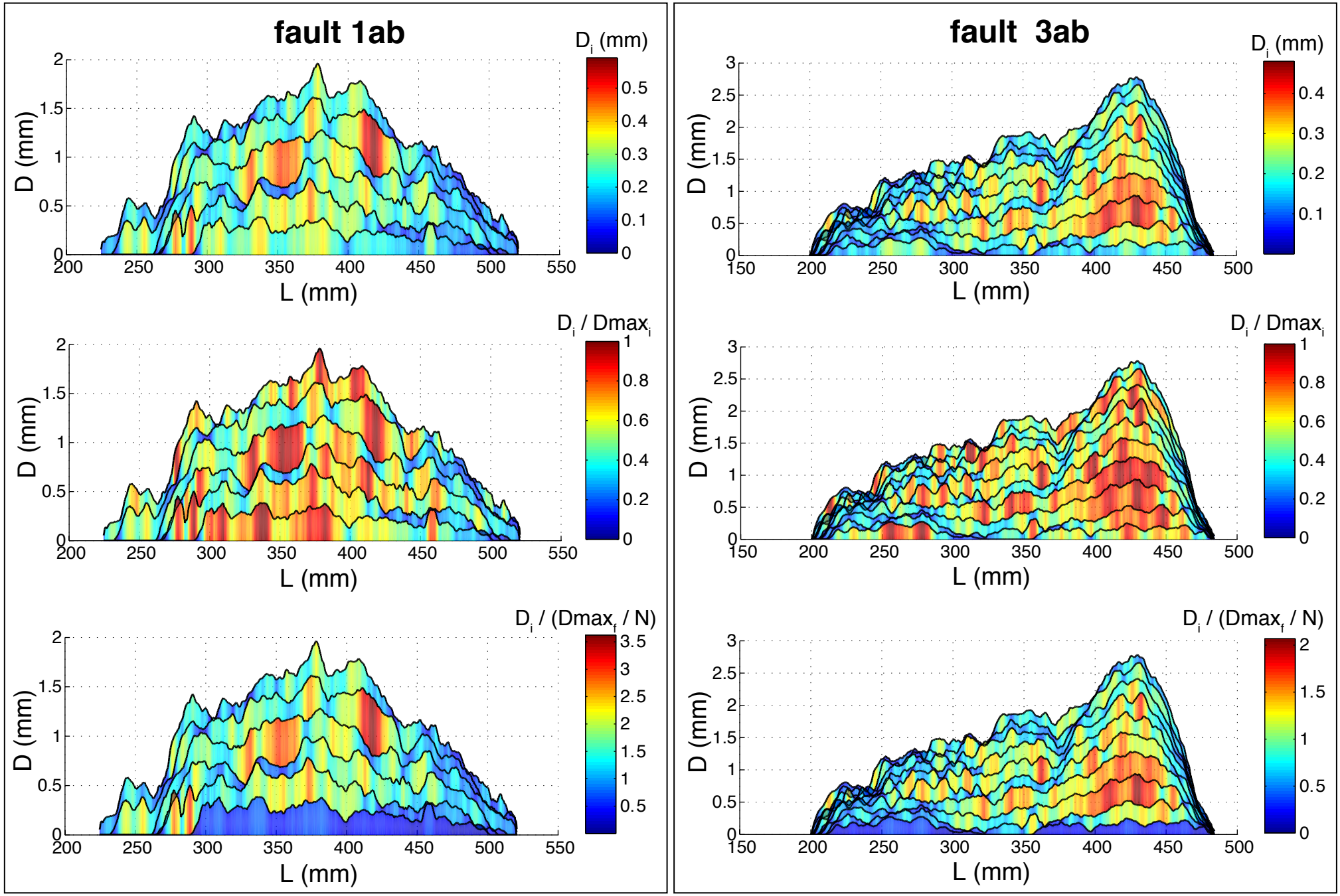

FIGURE 9 - Schlagenhauf et al.

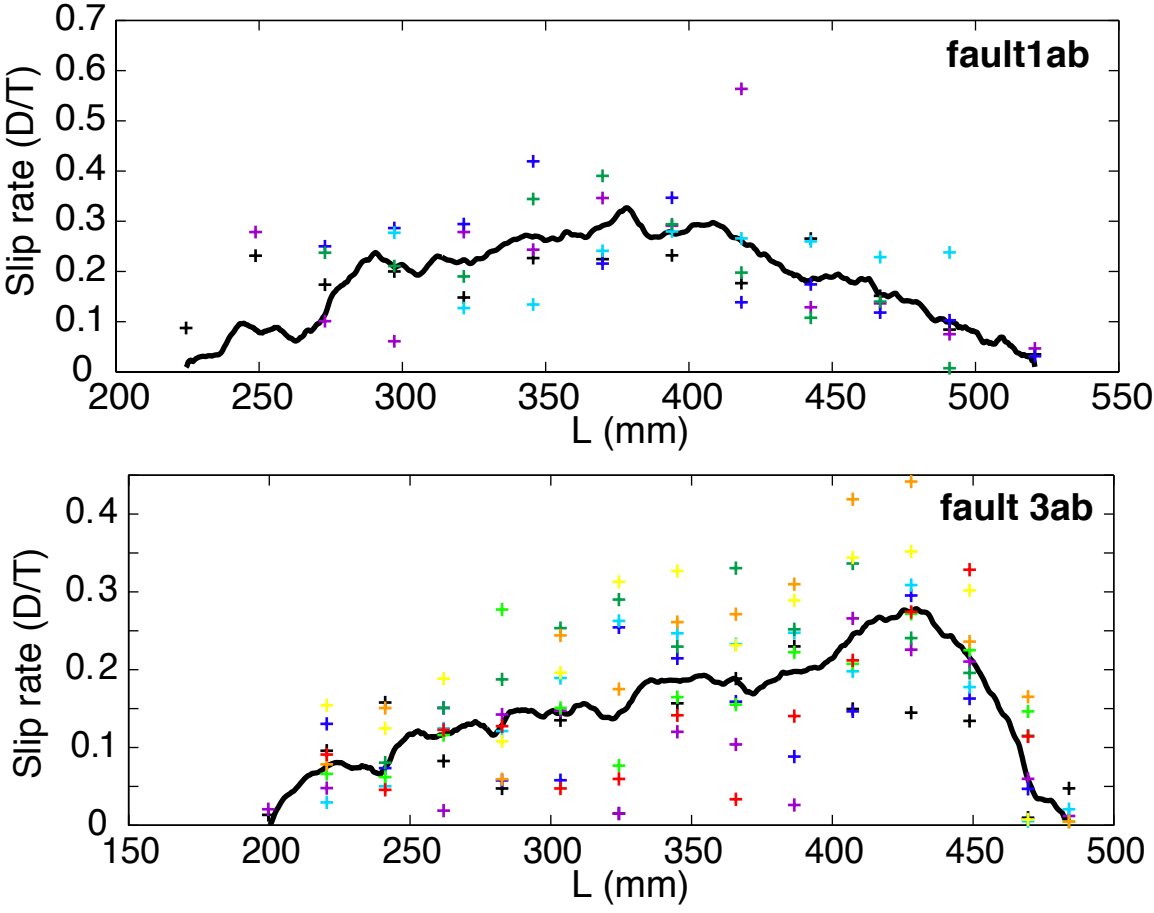

FIGURE 10 - Schlagenhauf et al.

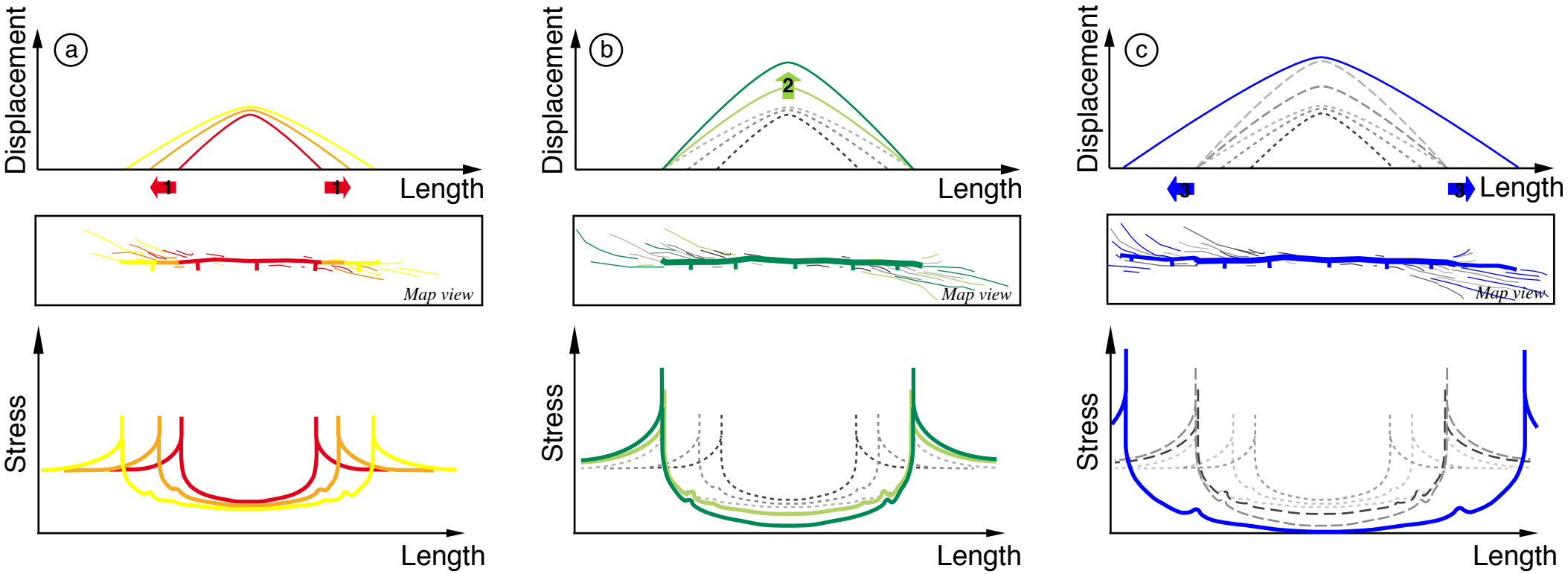

Ellec. Suppl. A,B,D,E,F,G,H,I + E.S. CAPTIONS

Click here to download Supplementary material for on-line publication only: SchlagenhaufEtAl_ELLECSUPPLandCAPTIONS.pdf

Ellec. Suppl. C (movie)

Click here to download Supplementary material for on-line publication only: SchlagenhaufEtAl_ES_C.mov